Soil & Environmental Health 3 (2025) 100148

Contents lists available at ScienceDirect

Soil & Environmental Health

journal homepage: www.sciencedirect.com/journal/soil-and-environmental-health

Research Paper

Role of permafrost thaw transitions in biogeochemical nitrogen cycling

Merritt N. Logan [a], Monique S. Patzner [b], Jacob P. VanderRoest [a], Bridget B. McGivern [a], Nivetha Srikanthan [c], Myrna J. Simpson [c], Amy M. McKenna [e,a], Kelly C. Wrighton [a], Casey Bryce [d], Andreas Kappler [b,f], Thomas Borch [a,*]

[a] Department of Soil & Crop Sciences and Department of Chemistry, Colorado State University, 307 University Ave, Fort Collins, CO 80523-1170, USA
[b] Geomicrobiology, Department of Geosciences, University of Tuebingen, Schnarrenbergstrasse 94-96, 72076 Tuebingen, Germany
[c] Environmental NMR Centre and Department of Physical & Environmental Sciences, University of Toronto Scarborough, Toronto, Ontario, M1C 1A4, Canada
[d] School of Earth Sciences, University of Bristol, Bristol, BS8 1RL, UK
[e] Ion Cyclotron Resonance Facility, National High Magnetic Field Laboratory, Florida State University, Tallahassee, FL 32310-4005, USA
[f] Cluster of Excellence EXC 2124: Controlling Microbes to Fight Infections, Tübingen, Germany

HIGHLIGHTS

- Permafrost thaw corresponds with a spike in dissolved organic N.
- Permafrost thaw fronts serve as transition zones with distinct dissolved organic N.
- Peptide-like organic N is limited at the point of permafrost collapse.
- Upregulated N-utilizing metabolomic pathways correlated to limited organic N in bog.

GRAPHICAL ABSTRACT

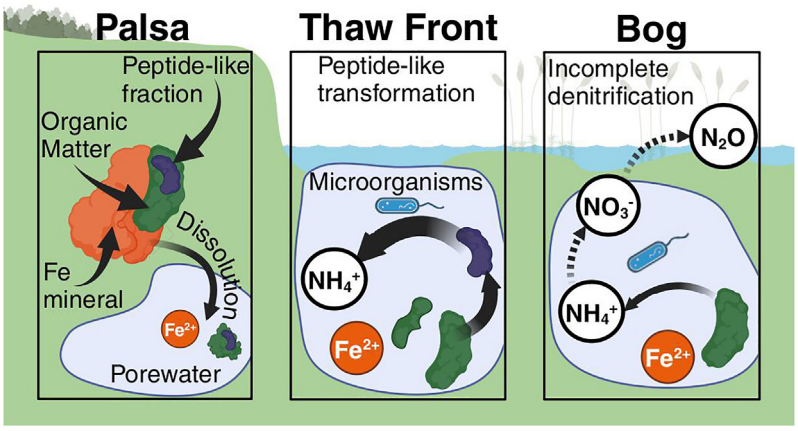

ARTICLE INFO

Handling Editor: Lena Q. Ma
Technical Editor: Lena Q. Ma

Keywords:
N dynamics
Climate change
Metatranscriptomics
Environmental health
Microbial activity changes
NMR and FT-ICR MS
Bog and peatlands

ABSTRACT

Significant organic nitrogen (ON) stocks have accumulated in permafrost peatlands over millennia. Climate change is expected to increase peatland thaw, making this ON more susceptible to biogeochemical degradation. However, the interplay between thaw-released N and N cycling remains poorly understood. To elucidate ON composition across a thaw transition (palsa to thaw front to bog), we employed 21 T electrospray ionization Fourier transform ion cyclotron resonance mass spectrometry (FT-ICR MS) and nuclear magnetic resonance (NMR) spectroscopy. In addition, we performed metatranscriptomic sequencing to evaluate microbial activity changes in N cycling pathways between the palsa and bog. We observed an approximate 10-fold increase in dissolved ON and a significant rise in ammonium concentration between the palsa and thaw front. Additionally, there was a reduction in the peptide-like fraction and an increase in the aromatic fraction of dissolved ON molecules. Dissolved ON concentrations decreased by 73 % between the thaw front and bog, while expression of

* Corresponding author.
E-mail addresses: merritt.logan@colostate.edu (M.N. Logan), thomas.borch@colostate.edu (T. Borch).

https://doi.org/10.1016/j.seh.2025.100148
Received 4 February 2025; Received in revised form 25 March 2025; Accepted 26 March 2025
Available online 28 March 2025

Palsa and thaw front
Dissolved organic N
Transcriptomic gene expression

ammonium-producing genes was significantly higher in the bog compared to the palsa. Our findings highlight the release and rapid compositional shift of ON during thaw transitions. This underscores the need for further studies on thaw-released N to enhance models predicting N cycling and Arctic greenhouse gas emissions.

1. Introduction

Approximately 15 % of land area in the northern hemisphere is underlain by permafrost, serving as a major sink for both carbon and nitrogen (Hugelius et al., 2014; Hugelius et al., 2020; Mishra et al., 2017; Obu, 2021; Schuur et al., 2013; Zhang et al., 2008). The northern circumpolar permafrost region stores an estimated 1600 Pg of carbon and 67 Pg of nitrogen accumulated over thousands of years in frozen or saturated anoxic soils, representing approximately 33 % and 50 % of the total global carbon and nitrogen stocks respectively (Batjes, 1996; Harden et al., 2012; Schuur et al., 2022; Voigt et al., 2017). Climate change is expected to release large quantities of these stocks as greenhouse gas (GHG), and between 1971 and 2019 warming in permafrost regions has increased two to four times faster than global averages, accelerating permafrost loss and environmental disturbances (Abbott et al., 2022; AMAP, 2021).

Permafrost peatlands, a subset of permafrost, cover ~3.7 million km^2 and store ~415 Pg of carbon and ~10 Pg of nitrogen (Harris et al., 1988; Holmes et al., 2022; Hugelius et al., 2020; Wilson et al., 2016). Many permafrost peatlands are especially susceptible to thawing as their average annual near-surface temperatures are within 1 °C of freezing (Jorgenson et al., 2001). Therefore, minimal warming can raise average annual temperatures above 0 °C, inducing thaw and exposing the stored organic carbon and nitrogen to biogeochemical mineralization (McGuire; et al., 2018; Schädel et al., 2014). This increased mineralization is expected to release substantial amounts of GHG, contributing to climate change and further accelerating thawing (Schuur et al., 2015). While many studies focus on carbon cycling and carbonaceous GHG (Cooper et al., 2017; Knoblauch et al., 2018; Schaefer et al., 2014), research on nitrogen cycling and nitrogenous GHG release is comparatively limited. However, the fate of organic nitrogen is drawing increased interest due in part to its potential transformation to N_2O (a greenhouse gas with a warming potential 298 times greater than CO_2 (Butterbach-Bahl et al., 2013; Hugelius et al., 2020; Marushchak et al., 2021; Voigt et al., 2017) and the important role that nitrogen plays in nutrient cycling.

Nitrogen availability and utilization in permafrost peatlands are influenced by seasonal thaw depth and thaw conditions (Fiencke et al., 2022; Harms and Jones, 2012; Norby et al., 2019; Walker et al., 2005). The active layer, which thaws each summer, varies in depth depending on seasonal conditions and temperature. Within this layer, the upper 5–15 cm contains lower nitrogen concentrations than deeper, perennially frozen soils. However, nitrogen bioavailability is limited by either restricted root access within the deeper active layer or by frozen conditions in the permafrost below (Keuper et al., 2012; Salmon et al., 2018). Research has demonstrated that active layer expansion of ~10 cm into permafrost can result in a sevenfold increase in dissolved inorganic nitrogen (DIN) release compared to seasonally thawed regions (Keuper et al., 2012; Salmon et al., 2018). Nitrogen inputs to peatlands through biological fixation and atmospheric deposition are relatively minor compared to stored nitrogen content (Ramm et al., 2022), despite varying with landscape and vegetation type. In permafrost systems, thaw events provide the primary source of nitrogen for biogeochemical cycling (Burke et al., 2022; Chen et al., 2018; Fiencke et al., 2022; Keuper et al., 2012).

Nitrogen cycling in terrestrial ecosystems involves complex interactions between organic and inorganic forms, mediated by microbial processes and environmental conditions (Kuypers et al., 2018). In permafrost systems, these cycles are particularly important as they influence ecosystem productivity and greenhouse gas emissions (Abbott and Jones, 2015; Marushchak et al., 2021; Patzner et al., 2022a). Recently, Ramm et al. (2022) proposed an updated model for nitrogen cycling within permafrost soils suggesting higher nitrogen cycling activity in seasonally thawed surface soils than previously presumed (Ramm et al., 2022). This model illustrates the relationships between organic nitrogen pools and the production of bioavailable nitrogen forms (ammonium, nitrate, and N_2). Their work indicates that while protein depolymerization rates are high, they do not directly control nitrogen turnover. Instead, dissolved organic nitrogen (DON) concentration during seasonal thawing appears to be the primary driver of inorganic nitrogen cycling (Ramm et al., 2022). Furthermore, the composition of the DON can affect ammonification and production of inorganic nitrogen; however, the controls of ammonification in thawing permafrost are still not well-studied (Fiencke et al., 2022; Ramm et al., 2022; Wegner et al., 2022; Wild et al., 2014). Soil conditions during thaw also affect inorganic nitrogen concentrations by influencing the activity of nitrogen cycling pathways (Fiencke et al., 2022; Voigt et al., 2020). For example, thaw transition studies have observed increased nitrate concentrations in thawed soil with moderate moisture (40–80 % water filled pore space) adjacent to existing permafrost. These studies suggest that increased nitrate concentrations could enhance N_2O emissions via denitrification, provided that an active nitrogen reducing microbial community is present (Mao et al., 2019; Wegner et al., 2022). Ultimately, nitrogen demand and fate in permafrost systems are controlled by the interplay of available ammonium, nitrification and denitrification activity, and soil moisture conditions. In permafrost peatlands, thaw creates distinct moisture interfaces that manifest as either thermokarst features or thaw slumps (Mao et al., 2019; Schuur et al., 2007; Wegner et al., 2022). When thaw occurs adjacent to bog areas, soil can collapse and become saturated depending on water table depth. In thaw slumps, rather than exhibiting the peat breakage characteristic of thermokarsts, the peat surface undergoes elevation loss while maintaining structural integrity (Varner et al., 2022). These thaw transitions represent zones of variable water saturation and rapidly shifting microbial communities and have been identified as potential hotspots of GHG release due to their fluctuating oxic and anoxic conditions (Elder et al., 2021; Fiencke et al., 2022; Wegner et al., 2022). However, to our knowledge, previous studies examining nitrogen dynamics across thaw transitions have not investigated fully saturated thawed soil conditions (Mao et al., 2019; Wegner et al., 2022), nor have they characterized the composition of the organic nitrogen pool (AminiTabrizi et al., 2020; Hodgkins et al., 2014; Hodgkins et al., 2016; Mann et al., 2015; Moore et al., 2023). Understanding biogeochemical nitrogen cycling within these dynamic thaw front environments requires detailed characterization of both the released organic nitrogen composition and the expression of microbial genes involved in nitrogen transformation pathways (Grosse et al., 2016; Ramm et al., 2022; Voigt et al., 2017).

Evaluating organic nitrogen composition within complex organic matter requires molecular-level analytical techniques capable of resolving tens of thousands of polyfunctional molecules. Such characterization demands a mass analyzer with high dynamic range, high sensitivity, and ultrahigh resolving power across a wide molecular weight range (m/z 150–1500) (Bahureksa et al., 2022; Smith et al., 2018). Fourier transform ion cyclotron resonance mass spectrometry (FT-ICR MS) uniquely meets these requirements, with the 21 T hybrid linear ion trap/FT-ICR mass analyzer achieving the highest resolving power to date (3,000,000 at m/z 200) (Bahureksa et al., 2022). The ultrahigh resolution of 21T FT-ICR MS enables accurate molecular formula assignments within complex dissolved organic matter (DOM) matrices

(Bahureksa et al., 2021; Hawkes and Kew, 2020; Nebbioso and Piccolo, 2013; Patzner et al., 2022a; Sleighter and Hatcher, 2007). This capability allows for post-analysis isolation of nitrogen-containing formulae, separating them from the larger, total DOM pool. Such isolation enhances our ability to track patterns of selective degradation or preservation of nitrogenous species that would otherwise be obscured in the total DOM pool. While FT-ICR MS has been successfully employed to study OM composition changes between bogs and fens and in laboratory incubation studies, it has not yet been applied to characterize organic nitrogen within a thaw front (Hodgkins et al., 2016; MacDonald et al., 2021; Stücheli et al., 2018; Textor et al., 2019; Wilson et al., 2022; Zherebker et al., 2019).

In this study, we examined the thaw transition from palsa to thaw front to bog, which represents the progressive stages of permafrost thaw. We present a molecular-level characterization of DON and inorganic nitrogen using electrospray ionization FT-ICR MS, NMR spectroscopy, and elemental analysis, allowing us to examine the changes in the composition of both organic and inorganic nitrogen and corroborate shifts in molecular structure. In addition, we complemented our chemical analysis by examining previously collected palsa and bog samples for the expression of genes associated with microbial nitrogen cycling pathways. Although these samples were collected during a separate field campaign than the porewater samples used for molecular and elemental analysis, the site conditions are highly comparable. This allowed us to evaluate the microbiome response in these distinct systems and provide a possible explanation for the biogeochemical shifts we observed. We hypothesized that (i) the thaw front will have elevated ammonium concentrations but not elevated nitrate concentrations due to wet, anoxic conditions, (ii) across the palsa-to-thaw front transition, peptide-like molecules will be depleted while aromatic molecules will be more abundant due to preferential microbial degradation, and (iii) the predominantly anoxic bog will not show increased microbial gene expression associated with denitrification due to nitrate limitations.

2. Materials and methods

2.1. Site description

Field sampling was conducted at Stordalen Mire (68 22′ N, 19 03′E), a subarctic peatland underlain by discontinuous permafrost in northern Sweden with peat depth between 1 and 3 m (Malmer et al., 2005). This site has been studied since the 1970s, with anthropogenic warming driving ecosystem changes through permafrost thaw (Holmes et al., 2022; Rosswall et al., 1975; Rosswall and Granhall, 1980). The site comprises three distinct ecosystems (palsa, bog, and fen), whose characteristics and boundaries have remained stable over time, as demonstrated through DOM and gas flux measurements (AminiTabrizi et al., 2020; Holmes et al., 2022; Lakomiec et al., 2021; Patzner et al., 2022a; Patzner et al., 2022; Varner et al., 2022; Wilson et al., 2022). Although at our sampling site the position of the thaw front has progressed into the palsa, the adjacent palsa and bog have been stable ecosystems since at least 2000 (Olefeldt and Roulet, 2012). Greenhouse gas emissions at Stordalen are primarily controlled by thaw state and saturation conditions rather than interannual variation, and ecosystem differences remain consistent interannually (Lakomiec et al., 2021; Varner et al., 2022). This temporal stability supports the validity of comparing our samples collected at different time points (cores in 2016; porewater in 2019 and 2022).

We selected Stordalen Mire because its palsa-to-bog thaw transition provides a well-defined system where the shift to waterlogged, anoxic conditions coincides with reductive dissolution of Fe(III) minerals and substantial DOC release and oxidation (Patzner et al., 2022a). The sampling location within the mire as well as a photo of the sampling site are shown in Fig. 1. The three dominant vegetation communities of the mire are (1) ericaceous and woody plants in palsa (intact permafrost); (2) *Sphagnum* spp., sedges, and shrubs in ombrotrophic peatland or bog

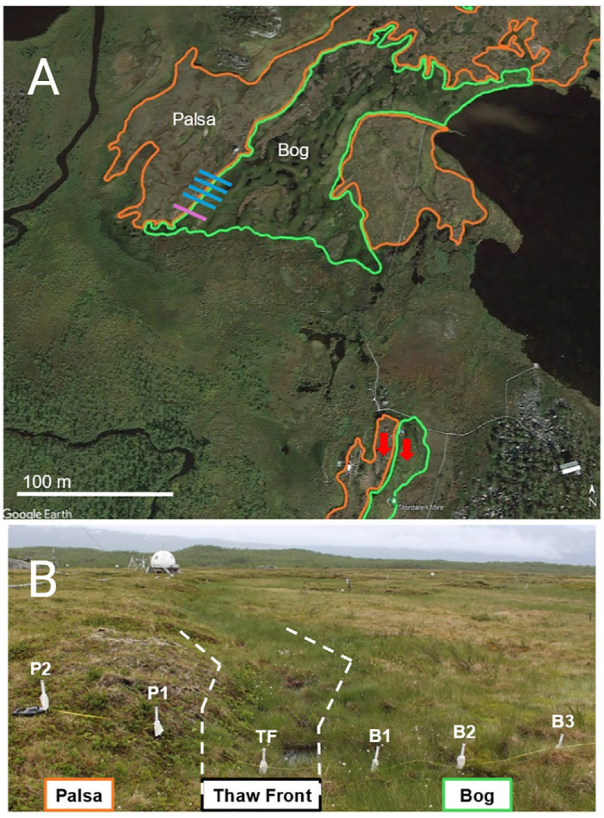

Fig. 1. (A) Stordalen mire, Abisko (Sweden) shown with palsa and bog regions. Transects 1–4 are shown as blue lines, transect 5 is shown as a purple line, and the soil cores used for metatranscriptome analysis are shown as red arrows. Palsa and bog regions are based on reported hydrological data (Holmes et al., 2022; Johansson et al., 2006; Olefeldt et al., 2012) and first hand observation during sampling. Maps data: Google Earth, CNES/Airbus, Lantmateriet/Metria, Maxar Technologies; copyright 2024. (B) Transect one lysimeters shown crossing the thaw transition. Palsa, thaw front, and bog regions in addition to sample points for transect one are shown. Dashed lines show thaw front moving away from the camera. Photo was taken looking north at 68°21′18.70″N, 19° 2′38.00″E.

(intermediate thaw); (3) sedges, mainly *Eriophorum* spp. in minerotrophic peatland or fen (full permafrost thaw) (Bäckstrand et al., 2010; Olefeldt et al., 2012).The palsa is oxic, features pH values of 4.5–5.5, and is elevated by underlying intact permafrost, leading to higher elevation than nearby bogs (Bockheim and Munroe, 2014; Payandi-Rolland et al., 2021). Bogs generally feature pH values of ~3.6, are waterlogged, and contain deep underlying permafrost (Fofana et al., 2022; Hodgkins et al., 2014, 2016; Olefeldt and Roulet, 2012).

2.2. Sample collection

Sampling was conducted along four transects incorporating the thaw transition (Fig. 2A). A fifth transect was collected 3 m adjacent to the initial sampling grid for inorganic and organic nitrogen content analysis. Transects 1–4 were collected in June/July 2019 and transect 5 was collected in September 2022. Transect locations were based on previously sampled palsa and bog locations (Patzner et al., 2020). Thaw front location was determined by measuring rapid reductive dissolution of reactive iron (III) (oxyhydr)oxide minerals due to soil saturation, releasing a pulse of aqueous Fe^{2+} (Patzner et al., 2022a). Therefore, the thaw front position was defined as the point in the transect with the highest $Fe^{2+}_{(aq)}$ concentration, correlating with the point of soil saturation. Due to natural variation in the thaw progression, the thaw front occurred at different points in our sampling transects (Fig. 2A). Based on

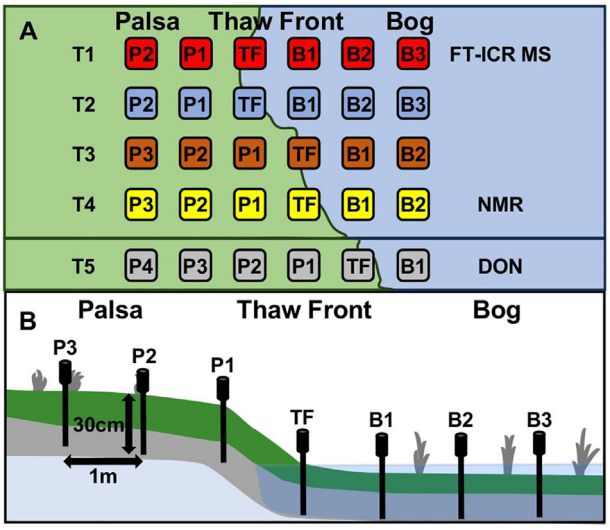

Fig. 2. (A) Top-down view of porewater sampling transects with sample points marked by thaw conditions along the transect. Palsa (P) and bog (B) are numbered according to their distance from the thaw front. The thaw front (TF) is identified as the point with the maximum $Fe^{2+}_{(aq)}$ concentration in each transect. Transects are labeled as T1-4 and are spaced 1 m apart. Transect 5 is located approximately 3 m to the south of T4 and crosses the same thaw transition. Transects 1–4 were used for elemental analysis. FT-ICR MS and NMR analyses were conducted on porewater from T1 and T4, respectively, and dissolved organic nitrogen (DON) was measured for T5. (B) Cross-section of porewater sampling within each transect showing sampling depth at 30 cm, lysimeters spaced every meter, permafrost collapse at the thaw front, and the approximate height of the water table in the bog. Green and gray layers comprise the active layer's primarily organic content and transition between organic and mineral horizons respectively. The light blue region shows permafrost ice.

thaw front location, the palsa (defined as intact permafrost) and the bog (opposing the palsa on the other side of the thaw front) were both labeled according to their respective distances from the thaw front (Fig. 2A). Porewater was collected along each transect at a depth of 30 cm, corresponding to the interface between the seasonally thawed active layer and the underlying perennially frozen permafrost, and consistently located within a transition zone between the organic and mineral horizons (Patzner et al., 2022a). Samples were labeled according to their position in the transect (Fig. 2B). The thawed-frozen interface serves as a lateral flow path, directing water from precipitation and active layer deepening from palsa to bog (Koch et al., 2013). Porewater was collected using lysimeters that were spaced 1 m apart along a given transect. The collected porewater was syringe filtered (0.22 μm) and transferred to dinitrogen-flushed SCHOTT bottles that were wrapped in aluminum foil to prevent photodegradation. The samples were then stored at 4 °C until further analysis, and sample volumes are reported in SI Table S1. Instrument access and sample volume limitations necessitated the use of select transects for FT-ICR MS and NMR, which are shown in Fig. 2A. Further description of porewater sampling can be found in previous work (Patzner et al., 2022a).

2.3. Porewater analysis

Total iron ($Fe_{(s)}$ and $Fe^{2+}_{(aq)}$) was measured by acidifying the porewater using 2 M HCl followed by a ferrozine assay and colorimetric analysis measured at 560 nm with further detail described in previous work (Patzner et al., 2022a; Patzner et al., 2020; Stookey, 1970). To measure DOC concentration, porewater was acidified with 2 M HCl to remove inorganic carbon and analyzed by total carbon analyzer (High TOC II, Elementar, Germany). Dissolved organic nitrogen was determined by measuring total nitrogen alongside DOC and subtracting inorganic nitrogen (Patzner et al., 2022a; Patzner et al., 2020; Treat et al., 2016). $Ammonium_{(aq)}$, $nitrate_{(aq)}$, and $nitrite_{(aq)}$ concentrations were measured with a flow injection analyzer (Seal Analytical, Germany) equipped with a dialysis membrane to remove $Fe^{2+}_{(aq)}$ and prevent side reactions during measurement. Due to sample volume limitations, nitrite and nitrate were analyzed in transects 1–4, DOC, $Fe^{2+}_{(aq)}$, and ammonium were analyzed in transects 1–5, and DON was analyzed in transect 5 (Table S2).

The mean analyte concentrations of the palsa samples (n = 13), thaw front samples (n = 5), and bog samples (n = 11) were statistically compared to each other. First, the normality of the analyte concentrations from each thaw state were evaluated using the Shapiro-Wilk test. If the populations of each thaw state were normally distributed, then the average analyte concentration of two thaw states were compared with the Welch's *t*-test. If one of the populations was not normally distributed, then the Mann-Whitney *U* test was used.

2.4. Nuclear magnetic resonance (NMR) spectroscopy

Nuclear magnetic resonance spectroscopy was utilized to determine the distribution of structural groups in total organic matter. Although ^{1}H NMR does not select for nitrogen containing compounds, it does provide an overview of the DOM chemistry that can be used for sample comparison with the corroborating molecular class abundances identified using FT-ICR MS (Bahureksa et al., 2021; Kim et al., 2022; Zark & Dittmar, 2018). Filtered (0.22 μm) porewater was lyophilized and yielded approximately 1 mg of freeze dried material. The freeze dried extracts were further dried over phosphorus pentoxide in a vacuum desiccator and then re-dissolved into 60 μL of deuterium oxide (D_2O, 99.9 % D) and 5 μL of sodium deuteroxide (NaOD, 99.5 % D, 30 wt % in D_2O). These dissolved samples were then centrifuged (10,000×*g* and 4 °C), and the supernatants were transferred into 1.7 mm NMR tubes (Norell). All samples were analyzed using a Bruker BioSpin Avance III 500 MHz NMR spectrometer (Karlsruhe, Germany) equipped with a ^{1}H–^{15}N–^{13}C TXI 1.7 mm microprobe with an actively shielded Z gradient. One-dimensional ^{1}H NMR spectra were collected using water suppression via pre-saturation utilizing relaxation gradients and, the spectra were collected using 2048 scans per sample with a recycle delay of 2 s and 32K time domain points. The spectra were processed using a zero-filling factor of two and were apodized by multiplication with an exponential decay corresponding to 0.3 Hz line broadening (Mitchell et al., 2018). NMR spectra were integrated based on typical DOM chemical shift regions associated with materials derived from linear terpenoids (MDLT; 0.6−1.6 ppm), carboxyl-rich alicyclic molecules (CRAM; 1.6−3.2 ppm), carbohydrates and peptides (3.2−4.5 ppm), and aromatic and phenolic components (6.5−8.4 ppm) (Mitchell et al., 2018; Woods and Simpson, 2011). The integration was performed using Analysis of Mixtures (AMIX; v. 3.9.15) software and expressed as percentage of the sum of the specific integration regions such that our comparison considered relative changes between these specific regions. It is important to note that some resonances (~1.9 ppm: likely from acetic acid; ~3.3 ppm likely from methanol; and ~8.4 ppm: likely from formic acid) (Mitchell et al., 2018; Tong et al., 2021; Woods and Simpson, 2011) do not align with the typical regions of DOM but were not excluded during integration due to overlapping resonances in some samples.

2.5. Metatranscriptome sequencing

Metatranscriptome sequencing was utilized to evaluate upregulation or downregulation of gene expression of enzymes in nitrogen cycling pathways, including but not limited to ammonification, nitrification, and denitrification. To survey microbial gene expression in Stordalen Mire, we used the genomes recovered in Woodcroft and Singleton et al. (Woodcroft et al., 2018). The 1529 metagenome-assembled genomes (MAGs) were dereplicated at 99 % identity with dRep (v2.6.2) (Olm et al., 2017) into 649 MAGs. The 99 % dereplicated MAGs were annotated with DRAM (v1.4.4)

(Shaffer et al., 2020). To assess the gene expression of these MAGs in the palsa and bog, we used metatranscriptome samples previously published in Ellenbogen et al. (2023). The metatranscriptomes derive from cores taken in July 2016 from defined palsa and bog environmental conditions at an adjacent thaw transition, and the thaw states have been well defined by previous work (Bäckstrand et al., 2010, 2008; Holmes et al., 2022; Johansson et al., 2006; Varner et al., 2022). We recognize the possibility of variability between the porewater transects and metatranscriptome peat cores. However, site restrictions prevented the collection of peat cores at the porewater thaw transition location. Furthermore, both sites represent well-defined thaw transitions in Stordalen Mire (Holmes et al., 2022). Additionally, the conditions of the palsa and bog are consistent at an interannual scale although there are year to year differences, the observed differences between them are consistent (AminiTabrizi et al., 2020; Wilson et al., 2022). Therefore, we are confident that the findings from the metatranscriptome analysis can be applied to the comparable porewater sampled from the palsa to bog transition. Soil cores were sectioned in the field at three depths: "surface" (1–4 cm), "middle" (10–14 cm), and "deep" (20–24 cm) and immediately put into LifeGuard (Qiagen). Metatranscriptome analysis used the deep section of the cores, as the 20–24 cm depth is most comparable to the 30 cm depth of porewater samples. Core sections were stored at −20 °C until analysis. DNA and RNA were co-extracted from 5 to 10 g peat using the Mobio PowerMax Soil DNA/RNA isolation kit (cat# 12966-10). Details on metatranscriptome library preparation, raw reads, gene annotation, and pathway expression comparison are provided in more detail in the SI (SI Section 1 and SI Data 1).

2.6. 21 T FT-ICR MS analysis

Fourier transform ion cyclotron resonance mass spectrometry assigns nitrogen-containing molecular formulae within the dissolved organic matter pool. The ability to segregate formulae according to elemental classes, like those that include nitrogen, enables us to differentiate compositional variations within each class that might otherwise be indiscernible within the total FT-ICR MS identified OM pool. Porewater DOM was analyzed with 21 T FT-ICR MS to identify and monitor DON compositional changes. Porewater was prepared for FT-ICR MS analysis by solid phase extraction (SPE) under N_2 atmosphere (glove bag) following a modified procedure based on Dittmar et al. (2008) and Li et al. (2016), which has been described in previous work (Patzner et al., 2022a; Patzner et al., 2020; Stücheli et al., 2018). The samples were processed under N_2 using degassed solvents to maintain the oxygen concentrations present *in situ*, and Hypersep Retain CX cartridges were selected for SPE due to reported improved nitrogen containing formulae and peptide-like formulae recovery compared to commonly used PPL cartidges (Stücheli et al., 2018). Hypersep Retain CX SPE cartridges (part# 60107-305, Thermo Fisher Scientific, Waltham, MA) were rinsed with 5 mL of HPLC grade methanol (Sigma-Aldrich, Rehovot, Israel) followed by 5 mL of 0.01 M HCl. Each DOM sample was acidified to pH ~2.5 and 0.5 mg C was loaded onto the SPE columns. After sample loading, the SPE cartridges were rinsed with 5 mL of 0.01 M HCl followed by drying with N_2 for 3–5 min. Finally, the samples were eluted with 1 mL of HPLC grade methanol and stored in airtight amber sample vials wrapped in aluminum foil at 4 °C. No additional dilution of the samples was performed prior to FT-ICR MS analysis.

Samples were analyzed as negative ions in a custom-built hybrid linear ion trap FT-ICR mass spectrometer equipped with a 21 T superconducting solenoid magnet (Hendrickson et al., 2015; Smith et al., 2018). Ionization conditions, instrument settings, and molecular formula assignment procedure are described in more detail in the SI (SI Section 2). The molecular formulae were assigned molecular class (condensed aromatic, aromatics/polyphenols, highly unsaturated, unsaturated aliphatic, saturated fatty acids, peptides, and sugars) according to the formula boundaries outlined by Poulin et al. (2017) (Table S3). For all mass spectra presented herein, between 10,024–11,357 mass peaks were assigned elemental compositions with root-mean-square mass measurement accuracy of 55–70 ppb with achieved resolving power of 3,400,000 at m/z 200. The *m/z* range including all samples was 165.0193–1155.211. Data processing post-formula assignment was performed with RStudio utilizing R software (V4.1.2). Table S4 shows the sample name, RMS error, and number of assignments for all spectra discussed herein. PetroOrg files, calibrated peak lists, and peak assignments are publicly available via the Open Science Framework via DOI 10.17605/OSF.IO/TZKWN.

3. Results

3.1. The thaw front featured the highest aqueous Fe^{2+}, DOC, ammonium, and DON concentrations

Transects 1–4 exhibited a pulse of $Fe^{2+}_{(aq)}$ and DOC at the saturated thaw front (Fig. 3A). Transect 5, which was collected to analyze DON concentrations, showed changes in concentration of $Fe^{2+}_{(aq)}$, ammonium, and DOC consistent with the previously sampled four transects, despite the 3-year gap in sampling time. The palsa, generally dry and oxic (Hodgkins et al., 2014), had the lowest levels of all measured species (Fig. 3 and Table S2). The only exception to this was nitrate, which had no statistically significant change between any of

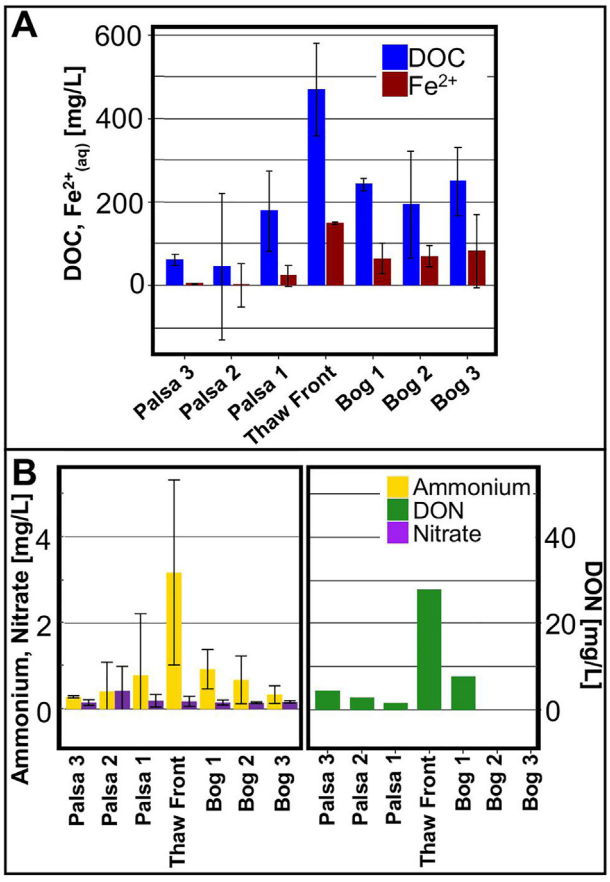

Fig. 3. Porewater composition across the thaw transition. (A) DOC and $Fe^{2+}_{(aq)}$ concentrations across the thaw transition. (B) Ammonium, nitrate, and DON concentrations across the thaw transition. Reported values and error bars represent the average and standard deviation of palsa-to-bog sampling transects. Error bars are not present for DON as only one transect (T5) was analyzed for DON, so n = 1 for all DON values. There were no DON values for Bog 2 and Bog 3 since there were no Bog 2 and Bog 3 sampling points for transect 5 due to the position of the thaw front. N-values for the remaining sample positions varied due to different thaw front positions in the transects (see Table S2 for full transect data).

the thaw states (Welch's *t*-test, $P > 0.05$) ranging between 1.27 and 0.07 mg/L. The thaw front had the highest concentrations of all analyzed species, with significantly higher levels (Welch's *t*-test, $P < 0.05$) of DOC and ammonium compared to the palsa and bog. The bog, which the palsa drains into via the thaw front (Olefeldt and Roulet, 2012), contained concentrations of ammonium that were not significantly different (Welch's *t*-test, $P > 0.05$) from the palsa. Similarly to ammonium, DON concentration decreased by 73 % immediately after the thaw front (Fig. 3B). Differences in DON concentrations could not be evaluated with Welch's *t*-test or the Mann-Whitney *U* test because DON was only measured along transect 5. Nevertheless, the thaw front DON concentration was substantially higher compared to other sampling points (10-fold increase compared to the average palsa concentration). Since the trends in DOC and $Fe^{2+}_{(aq)}$ are consistent across all transects when aligned to the pulse of $Fe^{2+}_{(aq)}$ (i.e., the thaw front), we can conclude that the geochemical profiles of the transects are comparable. Therefore, we propose that results from more detailed molecular analyses (FT-ICR MS and NMR) that were performed on select transects can be applied to the general thaw transition at Stordalen Mire.

3.2. *Thaw front DON has lower H/C and lower relative abundance of aliphatic formula compared to palsa and bog*

Van Krevelen diagram analysis showed clear compositional differences between the palsa and thaw front sites (Fig. 4A) The palsa (P2), thaw front, and bog (B3) featured 11272, 10852, and 10024 total monoisotopic formulae, respectively. Higher relative abundance formulae in the thaw front had lower H/C and higher O/C ratios and were more aromatic-like than in the palsa (Fig. 4A and B). Specifically, the percentage of aromatic/polyphenols-like and condensed aromatic-like formulae increased from 23 % in the palsa to 27 % in the thaw front followed by a decrease to 23 % in the bog. Higher aromatic-like content in the thaw front could be attributed to microbial degradation of polyphenolic compounds (Patzner et al., 2022a). Despite a 7.5-fold increase in DOC and a tenfold increase in the DON concentration at the thaw front, the number of identified DOC and DON formulae underwent minimal change. Assigned DON formulae represented approximately 27 % of the total formulae across all conditions. As observed in the total formulae, when only nitrogen-containing formulae (referred from here as CHNO formulae) were compared, the highly abundant CHNO formulae in the

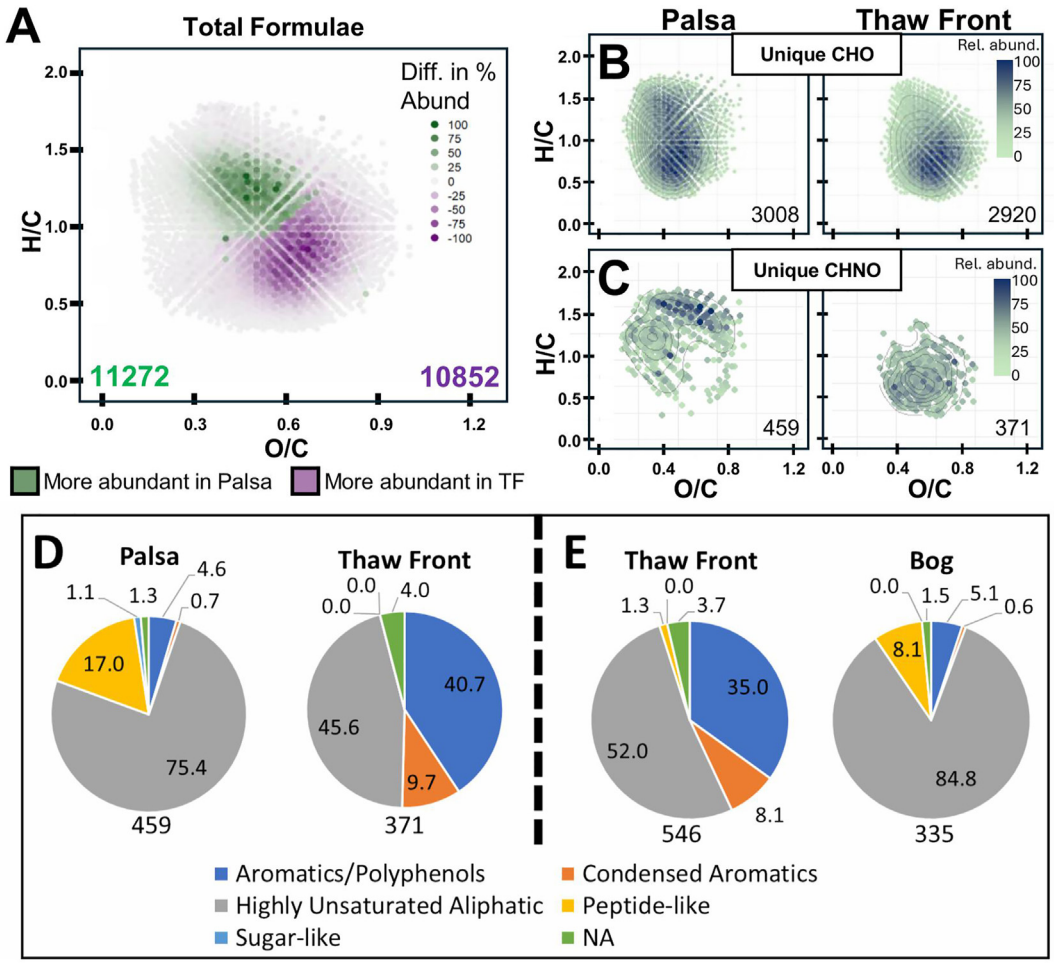

Fig. 4. Molecular formula characterization performed by FT-ICR MS of porewater samples. (A) Van Krevelen diagrams displaying comparisons between palsa (P2) and thaw front samples. Distribution of the total formula showing regions of higher abundance in palsa (green) and higher abundance in thaw front (purple). Color is determined by the difference in the relative abundance for a given formula between the palsa and the thaw front, with positive values having higher relative abundance in the palsa and negative values having higher relative abundance in the thaw front. The total count of identified formulae is inserted and color matched to palsa and thaw front. (B) Unique CHO formulae for palsa and thaw front and (C) unique CHNO formulae in palsa and thaw front colored by percent abundance of the formula. Inserted numbers in (B) and (C) are the number of formulae plotted in each plot. (D and E) Formula count of unique CHNO molecules shown as percentages of molecular class assigned by FT-ICR MS between (D) palsa (P2) and thaw front and (E) thaw front and bog (B3). The numbers of identified unique CHNO formulae for each thaw state are shown underneath each chart. Molecular class is defined by the heteroatom content of each molecular formula. Molecular class was defined according to Poulin et al. (2017). Unsaturated aliphatic and saturated fatty acid classes are not shown as there are no unique CHNO formulae in those classes.

thaw front also featured higher O/C and lower H/C ratios and were more aromatic-like than the palsa (Fig. 4C).

To further examine compositional differences in the assigned CHNO formulae, we isolated and compared formulae that were unique to each thaw state, hereafter referred to as the "unique pool". When comparing the unique CHNO pools between the palsa and thaw front, there is a clear compositional difference in CHNO formulae, which is distinct from the unique CHO pools. (Fig. 4B and C). Comparable to the total formulae pools, the unique CHNO formulae shifted from more aliphatic-like in the palsa to more aromatic-like in the thaw front. In the palsa, most unique CHNO formulae with high relative abundance feature H/C values around 1.5, with only a few formulae in the region of highest unique CHO. Conversely, the thaw front lacks unique formulae with H/C values near 1.5 but features a cluster of formulae in the more aromatic-like region, consistent with its unique CHO pool. The unique CHNO pools reveal a distinct pattern: many formulae found in the palsa are missing from the thaw front, and vice versa (Fig. 4C).

To determine which formulae contributed to the differences in the unique CHNO pools, we compared unique CHNO formulae by assigned molecular class (Table S3). The thaw front contained more aromatic-like and less peptide-like unique CHNO formulae when compared to either palsa or bog (Fig. 4D–Table S5). Notably, when comparing the palsa and thaw front, the proportion of unique CHNO formulae that were peptide-like decreased from 17 % to 0 %. Simultaneously, the aromatic/polyphenols-like and condensed aromatic-like formulae increased from 5 % to 50 %. Although the thaw front drains into the bog, the high proportions of condensed aromatic/polyphenol-like and low proportion of peptide-like unique CHNO formulae of the thaw front were not present in the bog. From the thaw front to the bog, the unique CHNO condensed aromatic and aromatic/polyphenol-like fraction decreased from 43 % to 6 %. Unique CHNO peptide-like formula increased from the thaw front to the bog, increasing from 1 % in the thaw front to 8 % in the bog, but did not return to palsa levels.

3.3. Carbohydrate- and peptide-like content was lowest at the thaw front

The FT-ICR MS results were complemented with solution-state ^{1}H NMR spectroscopy data to evaluate the molecular structure of porewater DOM throughout transect 4 (Fig. 5A, spectra shown in Fig. S1). The

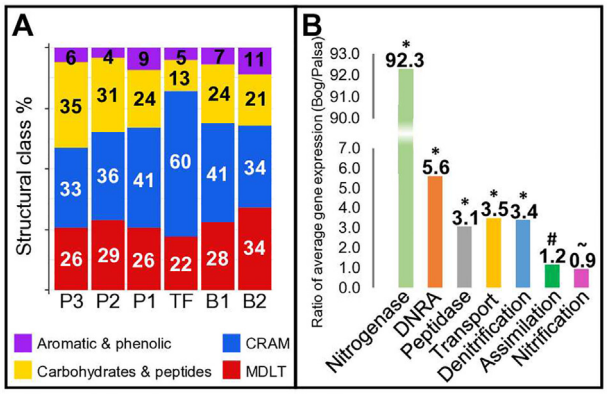

Fig. 5. (A) Relative abundance of general structural classes within porewater samples along the thaw transition determined by ^{1}H NMR. Sample position shown on the x-axis as P1-3 (palsa 1–3), TF (thaw front), B1-2 (bog 1–2). CRAM = carboxyl-rich alicyclic molecules, MDLT = materials derived from linear terpenoids. (B) Fold change in average metatranscriptome expression of microbial nitrogen cycling pathways between palsa (n = 3) and bog (n = 3) cores. The expression of pathways marked with (*) significantly (LIMMA, $p < 0.05$) increased, (#) increased but not significantly (LIMMA, $p > 0.05$), and (~) decreased but not significantly (LIMMA $p > 0.05$) when comparing gene expression in the bog to that in the palsa. Positive y-axis values indicate that the gene featured average greater expression in the bog than the palsa. See SI Data 1 for pathway information and statistics.

percentage of carbohydrates and peptides in the thaw front were approximately half of any other sample point (13 % in thaw front and 21–35 % in all other samples). The proportional decrease in carbohydrates and peptides correlated with a proportional increase in carboxylic rich alicyclic molecules (CRAM), considered an important product of microbial degradation (Hertkorn et al., 2006), which increased from 41 % in P1 to 60 % the thaw front. Like the FT-ICR MS results, the chemical composition in the thaw front did not persist into the bog. Notably the proportional CRAM content of the bog fell within the range of CRAM percentages in the palsa, and carbohydrate and peptide proportional content increased from thaw front to bog, although to only ~75 % of the palsa average. The remaining fractions, materials derived from linear terpenoids (MDLT) and aromatic/phenolic, featured nominal proportional changes across the thaw transition.

3.4. Microbial nitrogen cycling gene expression increased in the bog

To uncover the potential microbial processes contributing to nitrogen cycling in the palsa and bog, we mapped field metatranscriptome reads to a database of Stordalen Mire microbial metagenome assembled genomes (Woodcroft et al., 2018). We then aggregated genes into nitrogen cycling pathways and looked for altered gene expression levels between the palsa and bog (Fig. 5B–Supplementary Data 1). In the anoxic bog, several gene pathways were significantly upregulated (LIMMA, $p < 0.05$) including nitrogenase (*nifDKH*), dissimilatory nitrate reduction to ammonia (DNRA, *nrfA* and *nirBD*), nitrogen transporters, denitrification enzymes (*narGH, nirK, norB*), and peptidase pathways. Additionally, expression of genes in nitrogen assimilation (*nirA, nasA*) were upregulated in the bog but not to a significant extent (LIMMA, $p > 0.05$). Expression of nitrification (*hao*) was the only pathway to have lower expression in the bog than the palsa, but the decrease was not significant (LIMMA, $p > 0.05$).

4. Discussion

4.1. Thaw-induced conversion of DON to inorganic nitrogen

Several modeling studies suggest that the main factor controlling the production of inorganic nitrogen in thawing permafrost is the release of organic nitrogen (Hansen and Elberling, 2023; Ramm et al., 2022; Salmon et al., 2018). This release occurs due to the deepening of the active layer and the subsequent transformation of DON into ammonium (Lacroix et al., 2022; Mao et al., 2020; Ramm et al., 2022). When there is limited ammonium, which is the case for the active layer in most arctic soils, plant and microbial immobilization of nitrogen is dominant (Fiencke et al., 2022; Hansen and Elberling, 2023; Jones and Kielland, 2002; Salmon et al., 2018; Wegner et al., 2022). However, two *in situ* studies of permafrost thaw collapse linked DON release to elevated nitrate concentrations due to the improved drainage and oxic conditions after thaw (Mao et al., 2019; Wegner et al., 2022). Unlike these studies, the soil during and after the thaw front at our site remained saturated and at or below water level. At the thaw front we observed a large pulse of DON and significantly higher levels of ammonium compared to palsa and bog (Fig. 3). Despite the substantial ammonium within the thaw front, there was no significant change in nitrate concentrations across the thaw transition. In the well drained and oxic palsa, the limited nitrate is likely due to the low concentrations of DON and the lack of ammonium, which acts as substrate for nitrification. Conversely, in the thaw front and bog, the high saturation and anoxic conditions were likely the main limiters of nitrification (Fiencke et al., 2022; Kuypers et al., 2018; Olefeldt and Roulet, 2012; Wegner et al., 2022). Therefore, it is likely that the DON released during thaw is primarily mineralized to ammonium and any further nitrification is limited by the anoxic conditions. Our findings align with reported seasonal saturation of thaw slump floors, which observed increased ammonium concentrations and DON without

accumulating nitrate (Fiencke et al., 2022; Wegner et al., 2022). We propose that, confirming our first hypothesis, the high levels of ammonium within the thaw front are likely the result of rapid ammonification of DON.

4.2. Shifting composition of dissovled organic nitrogen at the thaw front

Within the thaw front, both NMR and FT-ICR MS results indicated the lowest proportions of peptide-like and carbohydrate molecules throughout the thaw transition (Figs. 3 and 4), despite a tenfold increase in DON concentration (Fig. 3). FT-ICR MS analysis of nitrogen-containing formulae showed the highest proportions of aromatics/polyphenols and condensed aromatics within the thaw front. NMR analysis of the total DOM pool revealed little change in aromatic and phenolic structures along the thaw transition, but it showed a substantial increase in CRAM structures at the thaw front. This increase likely reflects the overall oxidation and condensation of the DOM pool observed in previous studies (Patzner et al., 2022a), a pattern not captured in the nitrogen-specific FT-ICR MS analysis. The shift toward more condensed, less labile structures in both analyses, coupled with the decrease in peptide-like compounds, suggests active degradation of the nitrogen pool at the thaw front (D'Andrilli et al., 2015; Hertkorn et al., 2006). This interpretation aligns with soil amendment and incubation studies showing preferential mineralization of peptides and amino acids over larger nitrogen-containing organic molecules under conditions with abundant labile organic carbon (e.g., glucose) (Chen et al., 2018; Wild et al., 2013, 2014). Furthermore, arctic plant communities can preferentially uptake amino acids over nitrate, further increasing demand for labile DON (Jones and Kielland, 2002; Kielland, 1994; Schimel and Stuart Chapin, 1996; Wild et al., 2018). High nutrient demand in thaw fronts is expected as they have been identified as points of elevated microbial activity and active organic matter decomposition (Fiencke et al., 2022; Patzner et al., 2022a; Voigt et al., 2020). While we did not directly measure DON transformation, multiple lines of evidence suggest selective degradation is occurring. We observed a simultaneous decrease in labile peptide-like compounds and enrichment of less labile aromatic or cyclic molecules. This selective transformation of the DON pool parallels patterns documented in anoxic marine sediments, where peptides undergo selective deamination and microorganisms preferentially utilize free amino acids for cellular synthesis (Abdulla et al., 2018). The increased microbial activity previously reported at the thaw front (Patzner et al., 2022a; Patzner et al., 2022) would create higher demand for cellular building blocks, driving the observed depletion of available peptides. These findings confirm our second hypothesis and align with previous studies of permafrost nutrient cycling and DOC transformation (AminiTabrizi et al., 2020; Hodgkins et al., 2016; Mao et al., 2019; Ramm et al., 2022; Ward and Cory, 2015; Wild et al., 2014).

4.3. Organic nitrogen consumption at the thaw front leaves the bog nitrogen-limited

Metatranscriptomic data revealed an upregulation of gene expression for enzymes in nitrogen scavenging pathways in the bog (Fig. 5B). These pathways include nitrogen fixation, DNRA (a process often overlooked in permafrost studies) (Ramm et al., 2022), and mineralization via peptidases. Furthermore, in the water-saturated and anoxic bog, denitrification gene expression was significantly higher than in the palsa. Notably, we saw expression of genes encoding nitrate reductase (*narGH),* nitrite reductase (*nirK),* and nitric oxide reductase (*norB*) but not nitrous oxide reductase (*nosZ*), hinting that incomplete denitrification occurred in the bog. This could represent a pathway of nitrogen loss in the bog and N_2O generation, further contributing to nitrogen limitation (Ramm et al., 2022). However, saturated wetlands in the arctic have been found to have negligible N_2O emissions, due to the high water table acting as a diffusion barrier (Voigt et al., 2020). Anaerobic ammonia oxidation and complete ammonia oxidation could be additional pathways of nitrogen loss from the system, yet we did not detect gene expression for either of these processes.

At the thaw front, we observed a substantial increase in total DON concurrent with a reduction in the proportion of peptide-like molecular content. The adjacent bog showed a greater proportional decrease in DON concentration compared to DOC concentration (Fig. 3), indicating either preferential removal of nitrogen-containing molecules from solution or subsequent DOC release. This decrease in the proportion of nitrogen-containing organic matter in the bog corresponds with our metatranscriptomic results showing increased expression of nitrogen scavenging genes, suggesting a microbial response to reduced bioavailable DON.

After the pulse of ammonium at the thaw front, the anoxic conditions in the bog would limit nitrification, an aerobic process, which explains the persistence of low nitrate concentrations from thaw front to bog (Fig. 3). Furthermore, this limited nitrification would in turn limit denitrification by restricting production of nitrate (Fiencke et al., 2022; Voigt et al., 2020; Wegner et al., 2022). The observed decrease in DON, ammonium, and nitrate concentrations between the thaw front and bog suggests that the most labile and bioavailable nitrogen was likely transformed into ammonium and subsequently immobilized through biomass incorporation or removed though denitrification to N_2O (Kuypers et al., 2018; Voigt et al., 2017). However, contrary to our third hypothesis, denitrification increased in the bog despite the restricted nitrate substrate availability. This unexpected finding may reflect either increased denitrification activity or, more likely, upregulation of denitrification pathways as a mediating response to limited nitrate availability - similar to the upregulation of nitrogen scavenging pathways observed more broadly in the bog gene expression (Fig. 5). Although we did not collect metatranscriptome samples from the thaw front, our previous study documented increased activity of iron reducers and methanogens within it (Patzner et al., 2022a). Therefore, we propose the rapid appearance of high ammonium concentrations in this zone suggests similarly elevated nitrogen cycling activity, particularly ammonification. Although porewater and metatranscriptome samples were collected from different locations within Stordalen Mire, the consistent thaw conditions and ecology across sites (Holmes et al., 2022) allow these complementary datasets to inform our understanding of nitrogen transformations across the thaw transition.

4.4. Nitrogen availability is influenced by peptide content during permafrost thaw

Our data reveal an inverse relationship between peptide-like DON and ammonium concentrations along the permafrost thaw transition. At the thaw front, we observe depletion of labile peptide-like DON alongside enrichment of aromatic DON and elevated ammonium levels. In contrast, both the bog and palsa show higher peptide content with limited ammonium (Figs. 3–5). The consistent inverse relationship between peptide content and ammonium levels across sites suggests that peptide availability may act as a control point for nitrogen cycling, with peptide degradation regulating the ammonium pool available for subsequent nitrogen transformations. Although we did not directly measure nitrogen transformations at the thaw front, our metatranscriptomic analysis of the bog revealed increased expression of bioavailable nitrogen scavenging genes. These metatranscriptomic results support the role of microbial communities in driving nitrogen transformations at the thaw front. The relationship between nitrogen and carbon cycling in thawing permafrost remains poorly characterized, though nitrogen availability is expected to influence carbon mineralization and permafrost carbon feedback through both cellular synthesis and DOC mineralization priming (Abdulla et al., 2018; Schuur et al., 2022; Voigt et al., 2020). Based on our findings, we propose that components of Ramm's model (Ramm et al., 2022), particularly the controls on ammonification rates, can be applied to thaw fronts and bogs, with our suggested extensions illustrated in Fig. 6. Future studies directly examining metatranscriptomic activity at the thaw front will be crucial for fully understanding the fate of nitrogen-containing organic matter during permafrost thaw.

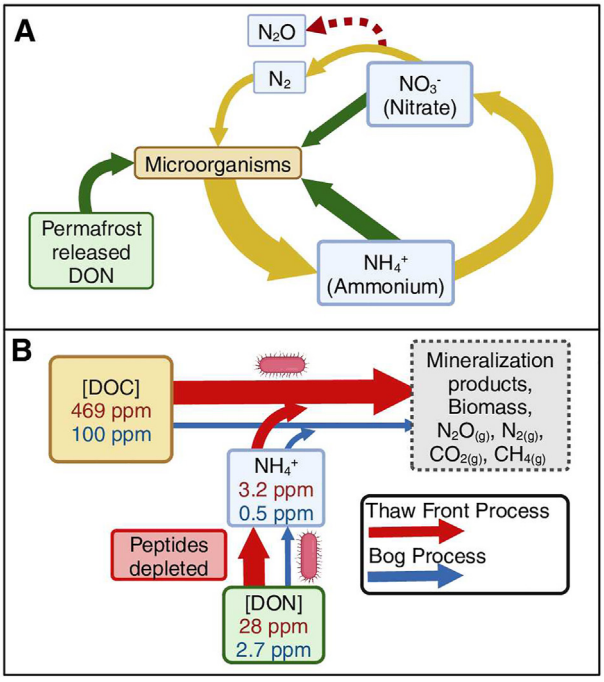

Fig. 6. (A) Modified conceptual model for nitrogen cycling within permafrost soils based on Ramm et al. (2022)(Ramm et al., 2022). Green arrows show uptake processes, yellow arrows show mineral N turnover processes, and red arrows show caseous losses. (B) Adapted model to show palsa vs. thaw front organic matter and nutrient transformation supported by empirical data reported herein. Data shows that high concentrations of organic nitrogen within the thaw front correlate to high ammonium concentrations and reduced peptide content. The production of ammonia can prime the microbial degradation of highly abundant DOC, potentially elevating the production of GHGs and biomass. Arrows are sized to indicate the expected relative amount of the transformation process based on previous GHG emission and nitrogen priming findings (Keuper et al., 2012; Mao et al., 2020; Voigt et al., 2017). Fig. 6(A) is based on Fig. 1 in "A review of the importance of mineral nitrogen …" by Ramm et al. (Ramm et al., 2022) and is licensed under a Creative Commons Attribution 4.0 International License (CC BY 4.0).

4.5. Conclusions

Our results provide some of the first detailed characterization of organic nitrogen dynamics within a permafrost thaw transition, revealing that the composition of organic nitrogen released during thaw significantly impacts nutrient cycling and creates biogeochemical hotspots within the thaw front environment. Notably, permafrost collapse and soil saturation resulted in high ammonium concentrations localized to the thaw front. Among nitrogen-containing molecules, the thaw front exhibited lower fractions of peptide and carbohydrate molecules and a higher fraction of aromatic molecules, aligning with previously reported selective degradation patterns of the total organic matter pool (Patzner et al., 2022a; Ramm et al., 2022; Wild et al., 2014). Nitrogen transformation during and after thaw appeared limited to DON mineralization, with no significant changes in nitrate concentration. However, the upregulation of denitrification under anoxic conditions in the bog suggests microbial metabolism could either contribute to N_2O emissions via incomplete denitrification (nitrate to N_2O) or mitigate N_2O release through complete denitrification (nitrate to N_2) (McGuire; et al., 2018; Mueller et al., 2015; Wegner et al., 2022). The absence of genes encoding N_2O reductase in the bog suggests thaw fronts may serve as previously underrepresented N_2O sources in climate models. Future studies combining metatranscriptome data from the thaw front with N_2O flux measurements would further elucidate nitrogen dynamics and improve our understanding of nitrogen mass balance in these systems. Our findings emphasize that future permafrost peatland studies and GHG models should incorporate thaw transitions due to their rapid and highly localized nitrogen dynamics.

CRediT authorship contribution statement

Merritt N. Logan: Writing – review & editing, Writing – original draft, Methodology, Investigation, Formal analysis, Conceptualization. **Monique S. Patzner:** Writing – review & editing, Methodology, Investigation, Conceptualization. **Jacob P. VanderRoest:** Writing – review & editing, Formal analysis. **Bridget B. McGivern:** Writing – review & editing, Methodology, Investigation, Formal analysis. **Myrna J. Simpson:** Writing – review & editing, Resources, Methodology, Investigation, Formal analysis. **Amy M. McKenna:** Writing – review & editing, Methodology, Investigation, Formal analysis, Conceptualization. **Kelly C. Wrighton:** Writing – review & editing, Methodology, Investigation, Funding acquisition, Formal analysis. **Casey Bryce:** Writing – review & editing, Resources, Project administration, Methodology, Investigation, Funding acquisition, Formal analysis, Conceptualization. **Andreas Kappler:** Writing – review & editing, Writing – original draft, Visualization, Supervision, Resources, Project administration, Methodology, Investigation, Funding acquisition, Formal analysis, Conceptualization. **Thomas Borch:** Writing – review & editing, Writing – original draft, Validation, Supervision, Project administration, Methodology, Investigation, Funding acquisition, Formal analysis, Conceptualization.

Data and code availability

All FT-ICR mass spectral data are publicly available through the Open Science Framework at DOI 10.17605/OSF.IO/TZKWN. R package used to process FT-ICR MS peak lists and produce figures is available at (https://github.com/robertyoung3/MSanalyzeNOM).

Funding sources

FT-ICR MS analyses were performed at the National High Magnetic Field Laboratory, which is supported by National Science Foundation Division of Chemistry and Division of Materials Research through Cooperative Agreement No. DMR-2128556 and the State of Florida. The sampling and field work conducted at the Abisko Scientific Research Station were made possible by The Swedish Polar Research Secretariat and The Swedish Infrastructure for Ecosystem Science (SITES). SITES is supported by the Swedish Research Council's grant 4.3-2021-00164. The authors acknowledge infra-structural support by the Deutsche Forschungsgemeinschaft (DFG, German Research Foundation) under Germany's Excellence Strategy, cluster of Excellence EXC2124, project ID 390838134. This work was supported by the University of Tuebingen (Programme for the Promotion of Junior Researchers award to Casey Bryce) and by the German Academic Scholarship Foundation (scholarship to Monique Patzner). The Natural Sciences and Engineering Research Council (NSERC) of Canada is thanked for their support via a Discovery Grant and the Tier 1 Canada Research Chair in Integrative Molecular Biogeochemistry to Myrna J. Simpson. Bridget B. McGivern and Kelly C. Wrighton were partially supported by awards from the National Science Foundation Biology Integration Institutes Program, Award #2022070, and from the Genomic Science Program of the United States Department of Energy Office of Biological and Environmental Research, award #DE-SC0023456. These funding sources had no role in the study design; collection, analysis and interpretation of data; in the writing of the report; and decision to submit the article for publication. Fig. 6 and graphical abstract were created with BioRender.com.

Declaration of Competing Interest

The authors declare the following financial interests/personal relationships which may be considered as potential competing interests: Andreas Kappler reports financial support was provided by German Research Foundation. Thomas Borch reports equipment, drugs, or supplies was provided by The National High Magnetic Field Laboratory, which is supported by National Science Foundation Division of Chemistry and Division of Materials Research through Cooperative Agreement No. DMR-2128556 and the State of Florida. Myrna Simpson reports financial support was provided by National Research Council Canada. Kelly Wrighton reports financial support was provided by National Science Foundation. If there are other authors, they declare that they have no known competing financial interests or personal relationships that could have appeared to influence the work reported in this paper.

Acknowledgements

We are especially grateful for the assistance of Jennie Wikström, Eric Lundin, Niklas Rakos, and Alexander Meire at the Abisko Scientific Research Station during the field campaign. We thank Eva Voggenreiter for her assistance collecting and analyzing porewater for DON concentrations after the completion of our campaign.

Appendix A. Supplementary data

Supplementary data to this article can be found online at https://doi.org/10.1016/j.seh.2025.100148.

References

Abbott, B.W., Jones, J.B., 2015. Permafrost collapse alters soil carbon stocks, respiration, CH4, and N2O in upland tundra. Glob. Change Biol. 21 (12), 4570–4587. https://doi.org/10.1111/gcb.13069.

Abbott, B.W., Brown, M., Carey, J.C., Ernakovich, J., Frederick, J.M., Guo, L., et al., 2022. We must stop fossil fuel emissions to protect permafrost ecosystems. Front. Environ. Sci. 10 (June), 1–13. https://doi.org/10.3389/fenvs.2022.889428.

Abdulla, H.A., Burdige, D.J., Komada, T., 2018. Accumulation of deaminated peptides in anoxic sediments of Santa Barbara Basin. Geochem. Cosmochim. Acta 223, 245–258. https://doi.org/10.1016/j.gca.2017.11.021.

AMAP, 2021. Arctic climate change update 2021: Key Trends and Impacts. Summary for Policy-makers. Arctic Monitoring and Assessment Programme (AMAP), Tromsø, Norway, p. 16.

AminiTabrizi, R., Wilson, R.M., Fudyma, J.D., Hodgkins, S.B., Heyman, H.M., Rich, V.I., et al., 2020. Controls on soil organic matter degradation and subsequent greenhouse gas emissions across a permafrost thaw gradient in northern Sweden. Front. Earth Sci. 8 (September). https://doi.org/10.3389/feart.2020.557961.

Bäckstrand, K., Crill, P.M., Jackowicz-Korczyński, M., Mastepanov, M., Christensen, T.R., Bastviken, D., 2010. Annual carbon gas budget for a subarctic peatland, Northern Sweden. Biogeosciences 7 (1), 95–108. https://doi.org/10.5194/bg-7-95-2010.

Bäckstrand, Kristina, Crill, P.M., Mastepanov, M., Christensen, T.R., Bastviken, D., 2008. Non-methane volatile organic compound flux from a subarctic mire in Northern Sweden. Tellus Ser. B Chem. Phys. Meteorol. 60 B (2), 226–237. https://doi.org/10.1111/j.1600-0889.2007.00331.x.

Bahureksa, W., Tfaily, M.M., Boiteau, R.M., Young, R.B., Logan, M.N., McKenna, A.M., Borch, T., 2021. Soil organic matter characterization by fourier transform ion cyclotron resonance mass spectrometry (fticr MS): a critical review of sample preparation, analysis, and data interpretation. Environ. Sci. Technol. 55 (14), 9637–9656. https://doi.org/10.1021/acs.est.1c01135.

Bahureksa, W., Borch, T., Young, R.B., Weisbrod, C., Blakney, G.T., McKenna, A.M., 2022. Improved dynamic range, resolving power, and sensitivity achievable with FT-ICR mass spectrometry at 21 T reveals the hidden complexity of natural organic matter. Anal. Chem. 94 (32), 11382–11389. https://doi.org/10.1021/acs.analchem.2c02377.

Batjes, N.H., 1996. Total carbon and nitrogen in the soils of the world. Eur. J. Soil Sci. 47, 151–163. https://doi.org/10.1111/j.1365-2389.1996.tb01386.x.

Bockheim, J.G., Munroe, J.S., 2014. Organic carbon pools and genesis of alpine soils with permafrost: a review. Arctic Antarct. Alpine Res. 46 (4), 987–1006. https://doi.org/10.1657/1938-4246-46.4.987.

Burke, E., Chadburn, S., Huntingford, C., 2022. Thawing permafrost as a nitrogen fertiliser: implications for climate feedbacks. Nitrogen 3 (2), 353–375. https://doi.org/10.3390/nitrogen3020023.

Butterbach-Bahl, K., Baggs, E.M., Dannenmann, M., Kiese, R., Zechmeister-Boltenstern, S., 2013. Nitrous oxide emissions from soils: how well do we understand the processes and their controls? Phil. Trans. Biol. Sci. 368 (1621). https://doi.org/10.1098/rstb.2013.0122.

Chen, H., Yang, Z., Chu, R.K., Tolić, N., Liang, L., Graham, D.E., et al., 2018. Molecular insights into arctic soil organic matter degradation under warming. Environ. Sci. Technol. 52, 4555–4564. https://doi.org/10.1021/acs.est.7b05469.

Cooper, M.D.A., Estop-Aragonés, C., Fisher, J.P., Thierry, A., Garnett, M.H., Charman, D.J., et al., 2017. Limited contribution of permafrost carbon to methane release from thawing peatlands. Nat. Clim. Change 7 (7), 507–511. https://doi.org/10.1038/nclimate3328.

D'Andrilli, J., Cooper, W.T., Foreman, C.M., Marshall, A.G., 2015. An ultrahigh-resolution mass spectrometry index to estimate natural organic matter lability. Rapid Commun. Mass Spectrom. 29 (24), 2385–2401. https://doi.org/10.1002/rcm.7400.

Dittmar, T., Koch, B., Hertkorn, N., Kattner, G., 2008. A simple and efficient method for the solid-phase extraction of dissolved organic matter (SPE-DOM) from seawater. Limnol Oceanogr. Methods 6 (6), 230–235. https://doi.org/10.4319/lom.2008.6.230.

Elder, C.D., Thompson, D.R., Thorpe, A.K., Chandanpurkar, H.A., Hanke, P.J., Hasson, N., et al., 2021. Characterizing methane emission hotspots from thawing permafrost. Glob. Biogeochem. Cycles 35 (12), 1–22. https://doi.org/10.1029/2020GB006922.

Ellenbogen, J.B., Borton, M.A., McGivern, B.B., Cronin, D.R., Hoyt, D.W., Freire-Zapata, V., et al., 2023. Methylotrophy in the Mire: direct and indirect routes for methane production in thawing permafrost. mSystems 9 (1). https://doi.org/10.1128/msystems.00698-23.

Fiencke, C., Marushchak, M.E., Sanders, T., Wegner, R., Beer, C., 2022. Microbiogeochemical traits to identify nitrogen hotspots in permafrost regions. Nitrogen 3 (3), 458–501. https://doi.org/10.3390/nitrogen3030031.

Fofana, A., Anderson, D., McCalley, C.K., Hodgkins, S., Wilson, R.M., Cronin, D., et al., 2022. Mapping substrate use across a permafrost thaw gradient. Soil Biol. Biochem. 175 (August), 108809. https://doi.org/10.1016/j.soilbio.2022.108809.

Grosse, G., Goetz, S., McGuire, A.D., Romanovsky, V.E., Schuur, E.A.G., 2016. Changing permafrost in a warming world and feedbacks to the Earth system. Environ. Res. Lett. 11 (4). https://doi.org/10.1088/1748-9326/11/4/040201.

Hansen, H.F.E., Elberling, B., 2023. Spatial distribution of bioavailable inorganic nitrogen from thawing permafrost. Glob. Biogeochem. Cycles 37 (2), 1–12. https://doi.org/10.1029/2022GB007589.

Harden, J.W., Koven, C.D., Ping, C.L., Hugelius, G., David McGuire, A., Camill, P., et al., 2012. Field information links permafrost carbon to physical vulnerabilities of thawing. Geophys. Res. Lett. 39 (15), 1–6. https://doi.org/10.1029/2012GL051958.

Harms, T.K., Jones, J.B., 2012. Thaw depth determines reaction and transport of inorganic nitrogen in valley bottom permafrost soils. Glob. Change Biol. 18 (9), 2958–2968. https://doi.org/10.1111/j.1365-2486.2012.02731.x.

Harris, S.A., French, H.M., Heginbottom, J.A., Johnston, G.H., Ladanyi, B., Sego, D.C., Everdingen, R.O., 1988. Glossary of Permafrost and Related Ground-Ice Terms Harris. Technical Memorandum (National Research Council of Canada. Associate Committee on Geotechnical Research). https://doi.org/10.4224/20386561.

Hawkes, J.A., Kew, W., 2020. High-resolution Mass Spectrometry Strategies for the Investigation of Dissolved Organic Matter. Multidimensional Analytical Techniques in Environmental Research. Elsevier Inc. https://doi.org/10.1016/b978-0-12-818896-5.00004-1.

Hendrickson, C.L., Quinn, J.P., Kaiser, N.K., Smith, D.F., Blakney, G.T., Chen, T., et al., 2015. 21 Tesla fourier transform ion cyclotron resonance mass spectrometer: a national resource for ultrahigh resolution mass analysis. J. Am. Soc. Mass Spectrom. 26 (9), 1626–1632. https://doi.org/10.1007/s13361-015-1182-2.

Hertkorn, N., Benner, R., Frommberger, M., Schmitt-kopplin, P., Witt, M., Kaiser, K., et al., 2006. Characterization of a Major Refractory Component of Marine Dissolved Organic Matter, vol. 70, pp. 2990–3010. https://doi.org/10.1016/j.gca.2006.03.021.

Hodgkins, S.B., Tfaily, M.M., McCalley, C.K., Logan, T.A., Crill, P.M., Saleska, S.R., et al., 2014. Changes in peat chemistry associated with permafrost thaw increase greenhouse gas production. Proc. Natl. Acad. Sci. USA 111 (16), 5819–5824. https://doi.org/10.1073/pnas.1314641111.

Hodgkins, Suzanne B., Tfaily, M.M., Podgorski, D.C., McCalley, C.K., Saleska, S.R., Crill, P.M., et al., 2016. Elemental composition and optical properties reveal changes in dissolved organic matter along a permafrost thaw chronosequence in a subarctic peatland. Geochem. Cosmochim. Acta 187, 123–140. https://doi.org/10.1016/j.gca.2016.05.015.

Holmes, M.E., Crill, P.M., Burnett, W.C., McCalley, C.K., Wilson, R.M., Frolking, S., et al., 2022. Carbon accumulation, flux, and fate in stordalen mire, a permafrost peatland in transition. Glob. Biogeochem. Cycles 36 (1). https://doi.org/10.1029/2021gb007113.

Hugelius, G., Strauss, J., Zubrzycki, S., Harden, J.W., Schuur, E.A.G., Ping, C.L., et al., 2014. Estimated stocks of circumpolar permafrost carbon with quantified uncertainty ranges and identified data gaps. Biogeosciences 11 (23), 6573–6593. https://doi.org/10.5194/bg-11-6573-2014.

Hugelius, Gustaf, Loisel, J., Chadburn, S., Jackson, R.B., Jones, M., MacDonald, G., et al., 2020. Large stocks of peatland carbon and nitrogen are vulnerable to permafrost thaw. Proc. Natl. Acad. Sci. U. S. A 117 (34), 20438–20446. https://doi.org/10.1073/pnas.1916387117.

Johansson, T., Malmer, N., Crill, P.M., Friborg, T., Åkerman, J.H., Mastepanov, M., Christensen, T.R., 2006. Decadal vegetation changes in a northern peatland, greenhouse gas fluxes and net radiative forcing. Glob. Change Biol. 12 (12), 2352–2369. https://doi.org/10.1111/j.1365-2486.2006.01267.x.

Jones, D.L., Kielland, K., 2002. Soil amino acid turnover dominates the nitrogen flux in permafrost-dominated taiga forest soils. Soil Biol. Biochem. 34 (2), 209–219. https://doi.org/10.1016/S0038-0717(01)00175-4.

Jorgenson, M.T., Racine, C.H., Walters, J.C., Osterkamp, T.E., 2001. Permafrost degradation and ecological changes associated with a warming climate in central Alaska. Clim. Change 48 (4), 551–579. https://doi.org/10.1023/A:1005667424292.

Keuper, F., van Bodegom, P.M., Dorrepaal, E., Weedon, J.T., van Hal, J., van Logtestijn, R.S.P., Aerts, R., 2012. A frozen feast: thawing permafrost increases plant-available nitrogen in subarctic peatlands. Glob. Change Biol. 18 (6), 1998–2007. https://doi.org/10.1111/j.1365-2486.2012.02663.x.

Kielland, K., 1994. Amino acid absorption by Arctic plants: implications for plant nutrition and nitrogen cycling. Ecology 75, 2373–2383. https://doi.org/10.2307/1940891.

Kim, S., Kim, D., Jung, M.J., Kim, S., 2022. Analysis of environmental organic matters by Ultrahigh-Resolution mass spectrometry—a review on the development of analytical methods. Mass Spectrom. Rev. 41 (2), 352–369. https://doi.org/10.1002/mas.21684.

Knoblauch, C., Beer, C., Liebner, S., Grigoriev, M.N., Pfeiffer, E., 2018. Methane production as key to the greenhouse gas budget of thawing permafrost. Nat. Clim. Change 8, 309–312. https://doi.org/10.1038/s41558-018-0095-z.

Koch, J.C., Ewing, S.A., Striegl, R., McKnight, D.M., 2013. Rapid runoff via shallow throughflow and deeper preferential flow in a boreal catchment underlain by frozen silt (Alaska, USA). Hydrogeol. J. 21 (1), 93–106. https://doi.org/10.1007/s10040-012-0934-3.

Kuypers, M.M.M., Marchant, H.K., Kartal, B., 2018. The microbial nitrogen-cycling network. Nat. Rev. Microbiol. 16 (5), 263–276. https://doi.org/10.1038/nrmicro.2018.9.

Lacroix, F., Zaehle, S., Caldararu, S., Schaller, J., Stimmler, P., Holl, D., et al., 2022. Mismatch of N release from the permafrost and vegetative uptake opens pathways of increasing nitrous oxide emissions in the high Arctic. Glob. Change Biol. 28 (20), 5973–5990. https://doi.org/10.1111/gcb.16345.

Lakomiec, P., Holst, J., Friborg, T., Crill, P., Rakos, N., Kljun, N., et al., 2021. Field-scale CH4 emission at a subarctic mire with heterogeneous permafrost thaw status. Biogeosciences 18 (20), 5811–5830. https://doi.org/10.5194/bg-18-5811-2021.

Li, Y., Harir, M., Lucio, M., Kanawati, B., Smirnov, K., Flerus, R., et al., 2016. Proposed guidelines for solid phase extraction of suwannee river dissolved organic matter. Anal. Chem. 88 (13), 6680–6688. https://doi.org/10.1021/acs.analchem.5b04501.

MacDonald, E.N., Tank, S.E., Kokelj, S.V., Froese, D.G., Hutchins, R.H.S., 2021. Permafrost-derived dissolved organic matter composition varies across permafrost end-members in the western Canadian Arctic. Environ. Res. Lett. 16 (2). https://doi.org/10.1088/1748-9326/abd971.

Malmer, N., Johansson, T., Olsrud, M., Christensen, T.R., 2005. Vegetation, climatic changes and net carbon sequestration in a North-Scandinavian subarctic mire over 30 years. Glob. Change Biol. 11 (11), 1895–1909. https://doi.org/10.1111/j.1365-2486.2005.01042.x.

Mann, B.F., Chen, H., Herndon, E.M., Chu, R.K., Tolic, N., Portier, E.F., et al., 2015. Indexing permafrost soil organic matter degradation using high-resolution mass spectrometry. PLoS One 10 (6), 1–16. https://doi.org/10.1371/journal.pone.0130557.

Mao, C., Kou, D., Wang, G., Peng, Y., Yang, G., Liu, F., et al., 2019. Trajectory of topsoil nitrogen transformations along a thermo-erosion gully on the Tibetan plateau. J. Geophys. Res.: Biogeosciences 124 (5), 1342–1354. https://doi.org/10.1029/2018JG004805.

Mao, C., Kou, D., Chen, L., Qin, S., Zhang, D., Peng, Y., Yang, Y., 2020. Permafrost nitrogen status and its determinants on the Tibetan Plateau. Glob. Change Biol. 26 (9), 5290–5302. https://doi.org/10.1111/gcb.15205.

Marushchak, M.E., Kerttula, J., Diáková, K., Faguet, A., Gil, J., Grosse, G., et al., 2021. Thawing Yedoma permafrost is a neglected nitrous oxide source. Nat. Commun. 12 (1). https://doi.org/10.1038/s41467-021-27386-2.

McGuire, A.D., Lawrence, D.M., Koven, C., Clein, J.S., Burke, E., Chen, G., et al., 2018. Dependence of the evolution of carbon dynamics in the northern permafrost region on the trajectory of climate change. Proc. Natl. Acad. Sci. USA 115 (15), 3882–3887. https://doi.org/10.1073/pnas.1719903115, 2.

Mishra, U., Drewniak, B., Jastrow, J.D., Matamala, R.M., Vitharana, U.W.A., 2017. Spatial representation of organic carbon and active-layer thickness of high latitude soils in CMIP5 earth system models. Geoderma 300, 55–63. https://doi.org/10.1016/j.geoderma.2016.04.017.

Mitchell, P.J., Simpson, A.J., Soong, R., Simpson, M.J., 2018. Nuclear magnetic resonance analysis of changes in dissolved organic matter composition with successive layering on clay mineral surfaces. Soil Systems 2 (1), 1–17. https://doi.org/10.3390/soils2010008.

Moore, M.R.N., Tank, S.E., Kurek, M.R., Taskovic, M., McKenna, A.M., Smith, J.L.J., et al., 2023. Ultrahigh resolution dissolved organic matter characterization reveals distinct permafrost characteristics on the Peel Plateau, Canada. Biogeochemistry (123456789). https://doi.org/10.1007/s10533-023-01101-3.

Mueller, C.W., Rethemeyer, J., Kao-Kniffin, J., Löppmann, S., Hinkel, K.M., Bockheim, J.G., 2015. Large amounts of labile organic carbon in permafrost soils of northern Alaska. Glob. Change Biol. 21 (7), 2804–2817. https://doi.org/10.1111/gcb.12876.

Nebbioso, A., Piccolo, A., 2013. Molecular characterization of dissolved organic matter (DOM): a critical review. Anal. Bioanal. Chem. 405 (1), 109–124. https://doi.org/10.1007/s00216-012-6363-2.

Norby, R.J., Slown, V.L., Iversen, C.M., Childs, J., 2019. Controls on fine-scale spatial and temporal variability of plant-available inorganic nitrogen in a polygonal tundra landscape. Ecosystems 22, 528–543. https://doi.org/10.1007/s10021-018-0285-6.

Obu, J., 2021. How much of the earth's surface is underlain by permafrost? J. Geophys. Res.: Earth Surf. 126 (5), 1–5. https://doi.org/10.1029/2021JF006123.

Olefeldt, D., Roulet, N.T., 2012. Effects of permafrost and hydrology on the composition and transport of dissolved organic carbon in a subarctic peatland complex. J. Geophys. Res.: Biogeosciences 117 (1), 1–15. https://doi.org/10.1029/2011JG001819.

Olefeldt, D., Roulet, N.T., Bergeron, O., Crill, P., Bäckstrand, K., Christensen, T.R., 2012. Net carbon accumulation of a high-latitude permafrost palsa mire similar to permafrost-free peatlands. Geophys. Res. Lett. 39 (3). https://doi.org/10.1029/2011GL050355.

Olm, M.R., Brown, C.T., Brooks, B., Banfield, J.F., 2017. DRep: a tool for fast and accurate genomic comparisons that enables improved genome recovery from metagenomes through de-replication. ISME J. 11 (12). https://doi.org/10.1038/ismej.2017.126.

Patzner, M., Logan, M., McKenna, A., Young, R., Zhou, Z., Joss, H., et al., 2022a. Microbial iron cycling during palsa hillslope collapse promotes greenhouse gas emissions before complete permafrost thaw. Communications Earth and Environment 3 (76). https://doi.org/10.1038/s43247-022-00407-8.

Patzner, M.S., Mueller, C.W., Malusova, M., Baur, M., Nikeleit, V., Scholten, T., et al., 2020. Iron mineral dissolution releases iron and associated organic carbon during permafrost thaw. Nat. Commun. 11 (1), 1–39. https://doi.org/10.1038/s41467-020-20102-6.

Patzner, M.S., Kainz, N., Lundin, E., Barczok, M., Smith, C., Herndon, E., et al., 2022. Seasonal fluctuations in iron cycling in thawing permafrost peatlands. Environ. Sci. Technol. https://doi.org/10.1021/acs.est.1c06937.

Payandi-Rolland, D., Shirokova, L.S., Labonne, F., Bénézeth, P., Pokrovsky, O.S., 2021. Impact of freeze-thaw cycles on organic carbon and metals in waters of permafrost peatlands. Chemosphere 279. https://doi.org/10.1016/j.chemosphere.2021.130510.

Poulin, B.A., Ryan, J.N., Nagy, K.L., Stubbins, A., Dittmar, T., Orem, W., et al., 2017. Spatial dependence of reduced sulfur in everglades dissolved organic matter controlled by sulfate enrichment. Environ. Sci. Technol. 51 (7), 3630–3639. https://doi.org/10.1021/acs.est.6b04142.

Ramm, E., Liu, C., Ambus, P., Butterbach-Bahl, K., Hu, B., Martikainen, P.J., et al., 2022. A review of the importance of mineral nitrogen cycling in the plant-soil-microbe system of permafrost-affected soils—changing the paradigm. Environ. Res. Lett. 17 (1), 013004. https://doi.org/10.1088/1748-9326/ac417e.

Rosswall, T., Granhall, U., 1980. Nitrogen cycling in a subarctic ombrotrophic mire. Ecol. Bull. (30), 63–95.

Rosswall, T., Flower-Ellis, J.G.K., Johansson, L.G., Jonsson, S., Rydén, B.E., Sonesson, M., 1975. Stordalen (abisko), Sweden. Ecol. Bull. (20), 265–294. Retrieved from. https://www.jstor.org/stable/45331782.

Salmon, V.G., Schädel, C., Bracho, R., Pegoraro, E., Celis, G., Mauritz, M., et al., 2018. Adding depth to our understanding of nitrogen dynamics in permafrost soils. J. Geophys. Res.: Biogeosciences 123 (8), 2497–2512. https://doi.org/10.1029/2018JG004518.

Schädel, C., Schuur, E.A.G., Bracho, R., Elberling, B., Knoblauch, C., Lee, H., et al., 2014. Circumpolar assessment of permafrost C quality and its vulnerability over time using long-term incubation data. Glob. Change Biol. https://doi.org/10.1111/gcb.12417.

Schaefer, K., Lantuit, H., Romanovsky, V.E., Schuur, E.A.G., Witt, R., 2014. The impact of the permafrost carbon feedback on global climate. Environ. Res. Lett. 9. https://doi.org/10.1088/1748-9326/9/8/085003.

Schimel, J.P., Stuart Chapin, F., 1996. Tundra plant uptake of amino acid and NH4+ nitrogen in situ: plants compete well for amino acid N. Ecology 77 (7), 2142–2147. https://doi.org/10.2307/2265708.

Schuur, E.A.G., Abbott, B.W., Bowden, W.B., Brovkin, V., Camill, P., Canadell, J.G., et al., 2013. Expert assessment of vulnerability of permafrost carbon to climate change. Clim. Change 119 (2), 359–374. https://doi.org/10.1007/s10584-013-0730-7.

Schuur, E.A.G., McGuire, A.D., Schädel, C., Grosse, G., Harden, J.W., Hayes, D.J., et al., 2015. Climate change and the permafrost carbon feedback. Nature 520 (7546), 171–179. https://doi.org/10.1038/nature14338.

Schuur, Edward A.G., Crummer, K.G., Vogel, J.G., MacK, M.C., 2007. Plant species composition and productivity following permafrost thaw and thermokarst in Alaskan tundra. Ecosystems 10 (2), 280–292. https://doi.org/10.1007/s10021-007-9024-0.

Schuur, Edward A.G., Abbott, B.W., Commane, R., Ernakovich, J., Euskirchen, E., Hugelius, G., et al., 2022. Permafrost and climate change: carbon cycle feedbacks from the warming arctic. Annu. Rev. Environ. Resour. 47, 343–371. https://doi.org/10.1146/annurev-environ-012220-011847.

Shaffer, M., Borton, M.A., McGivern, B.B., Zayed, A.A., La Rosa, S.L., Solden, L.M., et al., 2020. DRAM for distilling microbial metabolism to automate the curation of microbiome function. Nucleic Acids Res. 48 (16). https://doi.org/10.1093/nar/gkaa621.

Sleighter, R.L., Hatcher, P.G., 2007. The application of electrospray ionization coupled to ultrahigh resolution mass spectrometry for the molecular characterization of natural organic matter. J. Mass Spectrom. 42 (5), 559–574. https://doi.org/10.1002/jms.1221.

Smith, D.F., Podgorski, D.C., Rodgers, R.P., Blakney, G.T., Hendrickson, C.L., 2018. 21 Tesla FT-ICR mass spectrometer for ultrahigh-resolution analysis of complex organic Mixtures. Anal. Chem. 90 (3), 2041–2047. https://doi.org/10.1021/acs.analchem.7b04159.

Stookey, L.L., 1970. Ferrozine-A New Spectrophotometric Reagent for Iron, vol. 42, pp. 779–781. https://doi.org/10.1021/ac60289a016.

Stücheli, P.E., Niggemann, J., Schubert, C.J., 2018. Comparison of different solid phase extraction sorbents for the qualitative assessment of dissolved organic nitrogen in freshwater samples using FT-ICR-MS. J. Limnol. 77 (3), 400–411. https://doi.org/10.4081/jlimnol.2018.1791.

Textor, S.R., Wickland, K.P., Podgorski, D.C., Johnston, S.E., Spencer, R.G.M., 2019. Dissolved organic carbon turnover in permafrost-influenced watersheds of interior Alaska: molecular insights and the priming effect. Front. Earth Sci. 7 (October), 1–17. https://doi.org/10.3389/feart.2019.00275.

Tong, H., Simpson, A.J., Paul, E.A., Simpson, M.J., 2021. Land-use change and environmental properties alter the quantity and molecular composition of soil-derived dissolved organic matter. ACS Earth Space Chem. 5 (6), 1395–1406. https://doi.org/10.1021/acsearthspacechem.1c00033.

Treat, C.C., Wollheim, W.M., Varner, R.K., Bowden, W.B., 2016. Longer thaw seasons increase nitrogen availability for leaching during fall in tundra soils. Environ. Res. Lett. 11 (6). https://doi.org/10.1088/1748-9326/11/6/064013.

Varner, R.K., Crill, P.M., Frolking, S., McCalley, C.K., Burke, S.A., Chanton, J.P., et al., 2022. Permafrost thaw driven changes in hydrology and vegetation cover increase trace gas emissions and climate forcing in Stordalen Mire from 1970 to 2014. Phil. Trans. Math. Phys. Eng. Sci. 380 (2215). https://doi.org/10.1098/rsta.2021.0022.

Voigt, C., Marushchak, M.E., Lamprecht, R.E., Jackowicz-Korczyński, M., Lindgren, A., Mastepanov, M., et al., 2017. Increased nitrous oxide emissions from Arctic peatlands after permafrost thaw. Proc. Natl. Acad. Sci. U. S. A 114 (24), 6238–6243. https://doi.org/10.1073/pnas.1702902114.

Voigt, C., Marushchak, M.E., Abbott, B.W., Biasi, C., Elberling, B., Siciliano, S.D., et al., 2020. Nitrous oxide emissions from permafrost-affected soils. Nat. Rev. Earth Environ. 1 (8), 420–434. https://doi.org/10.1038/s43017-020-0063-9.

Walker, D.A., Raynolds, M.K., Daniels, F.J.A., Einarsson, E., Elvebakk, A., Gould, W.A., et al., 2005. The circumpolar Arctic vegetation map. J. Veg. Sci. 16, 267–282. https://doi.org/10.1111/j.1654-1103.2005.tb02365.x.

Ward, C.P., Cory, R.M., 2015. Chemical composition of dissolved organic matter draining permafrost soils. Geochem. Cosmochim. Acta 167, 63–79. https://doi.org/10.1016/j.gca.2015.07.001.

Wegner, R., Fiencke, C., Knoblauch, C., Sauerland, L., Beer, C., 2022. Rapid permafrost thaw removes nitrogen limitation and rises the potential for N2O emissions. Nitrogen 3 (4), 608–627. https://doi.org/10.3390/nitrogen3040040.

Wild, B., Schnecker, J., Capek, P., Guggenberger, G., Hofhansl, F., Kaiser, C., et al., 2013. Nitrogen dynamics in turbic cryosols from siberia and Greenland c. Soil Biol. Biochem. 67, 85–93. https://doi.org/10.1016/j.soilbio.2013.08.004.

Wild, B., Schnecker, J., Alves, R.J.E., Barsukov, P., Bárta, J., Čapek, P., et al., 2014. Input of easily available organic C and N stimulates microbial decomposition of soil organic matter in arctic permafrost soil. Soil Biol. Biochem. https://doi.org/10.1016/j.soilbio.2014.04.014.

Wild, B., Alves, R.J.E., Bárta, J., Čapek, P., Gentsch, N., Guggenberger, G., et al., 2018. Amino acid production exceeds plant nitrogen demand in Siberian tundra. Environ. Res. Lett. 13 (3). https://doi.org/10.1088/1748-9326/aaa4fa.

Wilson, R.M., Hopple, A.M., Tfaily, M.M., Sebestyen, S.D., Schadt, C.W., Pfeifer-Meister, L., et al., 2016. Stability of peatland carbon to rising temperatures. Nat. Commun. 7, 13723. https://doi.org/10.1038/ncomms13723.

Wilson, Rachel M., Hough, M.A., Verbeke, B.A., Hodgkins, S.B., Chanton, J.P., Saleska, S.D., et al., 2022. Plant organic matter inputs exert a strong control on soil organic matter decomposition in a thawing permafrost peatland. Sci. Total Environ. 820, 152757. https://doi.org/10.1016/j.scitotenv.2021.152757.

Woodcroft, B.J., Singleton, C.M., Boyd, J.A., Evans, P.N., Emerson, J.B., Zayed, A.A.F., et al., 2018. Genome-centric view of carbon processing in thawing permafrost. Nature 560 (7716), 49–54. https://doi.org/10.1038/s41586-018-0338-1.

Woods, G., Simpson, A., 2011. HILIC-NMR: toward the identification of individual molecular components in dissolved organic matter. Environ. Sci. Technol. 45 (13), 5910. https://doi.org/10.1021/es201716u.

Zark, M., Dittmar, T., 2018. Universal molecular structures in natural dissolved organic matter. Nat. Commun. 9 (1), 1–8. https://doi.org/10.1038/s41467-018-05665-9.

Zhang, T., Barry, R.G., Knowles, K., Heginbottom, J.A., Brown, J., 2008. Statistics and characteristics of permafros and ground-ice distribution in the Northen Hemisphere. Polar Geogr. 23 (2), 132–154. https://doi.org/10.1080/10889370802175895.

Zherebker, A., Podgorski, D.C., Kholodov, V.A., Orlov, A.A., Yaroslavtseva, N.V., Kharybin, O., et al., 2019. The molecular composition of humic substances isolated from yedoma permafrost and alas cores in the eastern siberian arctic as measured by ultrahigh resolution mass spectrometry. J. Geophys. Res.: Biogeosciences. https://doi.org/10.1029/2018jg004743.